Optimized epitaxial growth of Fe on Ag(001)

D. E. Bürgler,* C. M. Schmidt, D. M. Schaller, F. Meisinger, R. Hofer, and H.-J. Güntherodt
Institut für Physik, Universität Basel, Klingelbergstrasse 82, CH-4056 Basel, Switzerland
(Received 27 January 1997)

We report on a comprehensive study of the growth of 5-nm-thick epitaxial Fe(001) films on Ag(001) substrates which are deposited on Fe-precovered GaAs(001) wafers. We characterize the films *in situ* by scanning tunneling microscopy, low-energy electron diffraction, X-ray photoelectron spectroscopy, and depth profiling to obtain information about the geometrical and chemical surface structure. We find that the surface morphology is improved by either growing or postannealing the films at elevated temperatures. During deposition at and above room temperature, however, an atomic exchange process is activated that results in a thin Ag film (up to 1 ML) ''floating'' on top of the growing Fe film. We propose and confirm a growth procedure that yields clean, Ag-free surfaces with a morphology superior to the other films. This optimized recipe consists of two steps: (i) low-temperature growth of the first 2 nm in order to form a diffusion barrier for the Ag substrate atoms, and (ii) high-temperature deposition of the final 3 nm to take advantage of the improved homoepitaxial growth quality of Fe at elevated temperatures. The relevance of these results with respect to magnetic properties of multilayers is discussed. [S0163-1829(97)00431-1]

I. INTRODUCTION

Thin magnetic films and multilayers have recently attracted a lot of interest because they exhibit fascinating properties such as perpendicular anisotropy in thin films or giant magnetoresistance (GMR) and magnetic interlayer coupling in multilayers. These effects have their origin in special artificially grown structures and are inevitably closely related to the details of these structures.[1,2] Knowledge of structural details—both, from the morphological and chemical point of view—is needed for the understanding and modeling of these phenomena.

The subject of this work are 5-nm-thick epitaxial Fe(001) films grown on Ag(001). We aim to correlate the morphological and chemical properties at the surface to the growth conditions in order to develop an optimized preparation procedure with respect to chemical cleanness and surface flatness. Such a recipe is highly desired because the Fe/Ag film-substrate combination is often employed in magnetic multilayers and sandwich structures, which are widely used to study GMR, magnetic interlayer coupling and other magnetic properties.[3–6] In Fe/X/Fe (X=Ag, Au, Cr, etc.) sandwich samples, for instance, the surface characteristics of the Fe film which is to be covered by the spacer layer influence important quantities such as roughness and intermixing at the Fe/X interface, and thus they have a direct impact on the magnetic properties of the whole triplelayer. The dependence of the interlayer coupling on the growth conditions has been demonstrated experimentally for an Fe/Cr/Fe/Ag(001) system[7] which was similarly prepared to our samples. The effect of interface roughness (or spacer layer thickness fluctuations, which are related to the roughness of both involved interfaces) and chemical imperfections on the magnetic interlayer coupling and GMR have theoretically been studied by various authors.[8–13] Biquadratic coupling, for instance, is explained by some models to occur solely due to interface roughness[8,10] or paramagnetic impurities.[9] Thus, detailed information about the geometrical and chemical order at the interfaces is essential to explore the relevance of these models.

We employ a combination of molecular beam epitaxy (MBE), direct space imaging by scanning tunneling microscopy (STM) and chemical analysis by electron spectroscopy methods to directly obtain information about relationships between preparation procedure, morphology, and chemical composition at the surface.

The paper is organized as follows: Information about instrumentation and experimental procedures is given in Sec. II. In Sec. III we introduce the layer structure of our samples and characterize the Ag(001) substrates. Section IV deals with the morphological properties of as-grown and postannealed Fe films deposited either at room temperature (RT) or at 520 K (HT for high temperature), and in Sec. V we investigate their chemical properties. Aiming for growth optimization we propose and test in Sec. VI other growth scenarios involving growth at 100 K (LT for low temperature) or at low *and* high temperature (hereafter called MT for mixed temperature).[14] Finally we discuss the results in Sec. VII.

II. EXPERIMENT

All experiments are performed in a multichamber ultrahigh vacuum (UHV) system that provides a variety of facilities for sample preparation and characterization including MBE, ion-etching, STM, low-energy electron diffraction (LEED), scanning Auger electron spectroscopy (AES), and x-ray and ultraviolet photoelectron spectroscopy (XPS, UPS). The base pressure of the whole apparatus is in the 10^{-11} mbar range. Cycles of material removal by ion-etching with Ar^+ ions and subsequently monitoring the chemical composition of the residual surface by XPS are used to obtain depth profiles. The samples are clamped mechanically on holders made from tantalum which can be moved throughout the UHV system to all preparation and characterization tools mentioned above. For thermal treatments these sample holders can be inserted into a copper

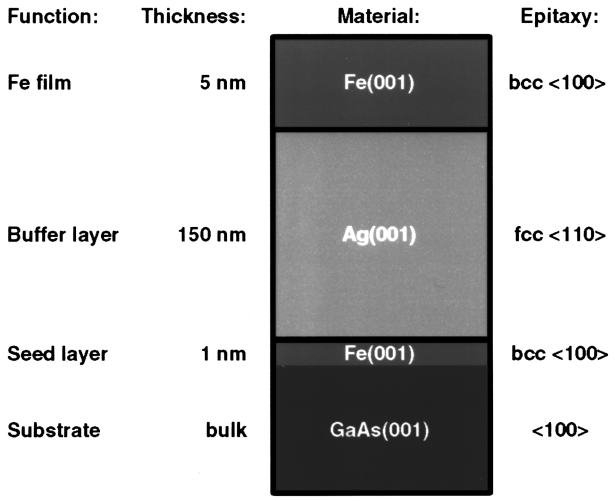

FIG. 1. Layer structure of the samples. Parallel aligned crystallographic axes in the surface plane defining the epitaxial relationships are given on the right hand side.

socket which is heated by a tungsten filament or cooled by liquid nitrogen. All indicated preparation temperatures are corrected for the temperature difference between the sample surface and the position of the thermocouple inside the copper socket yielding an absolute accuracy of ± 10 K. All morphological and chemical characterizations are performed at room temperature. More details about the instrumentation are given in Ref. 15.

The Fe films are deposited by means of an electron beam evaporator and their thickness is controlled by a quartz microbalance. We use a deposition rate of about 0.01 nm/s and vary the substrate temperature T_S in the range from 100 K to 570 K, whereas the film thickness is kept constant at 5 nm for all samples discussed in this paper. The background pressure during deposition typically is in the low 10^{-9} mbar range. Residual gas analysis by mass spectroscopy shows a strongly increased relative H_2 partial pressure during the operation of the evaporator independent of the material deposited. We attribute this to electron-stimulated desorption of hydrogen from the environment of the evaporator.

III. Ag(001) SUBSTRATE

The layer structure of our samples is shown in Fig. 1. Details about the preparation of the epitaxial Ag(001) buffer layers—the substrates of the Fe films discussed herein— are given in Ref. 15. Briefly, it consists of the following steps: (i) annealing the GaAs(001) wafer at the maximum temperature $T_A = 870$ K until a $(4\times n)$ LEED pattern indicates an ordered surface, (ii) deposition of an 1 nm Fe seed layer at a substrate temperature $T_S = 380$ K, (iii) deposition of a 150 nm Ag buffer layer at $T_S = 380$ K, and (iv) postannealing at $T_A = 570$ K. The final annealing temperature turns out to be critical as Ga atoms diffuse to the Ag surface above 620 K.[15] For $T_A = 570$ K, however, the epitaxial Ag(001) buffer layer is free of contaminants as checked by STM, AES, XPS, and UPS.

Figure 2(a) shows an STM image of the Ag(001) buffer layer after postannealing at $T_A = 570$ K. Many curved single atomic steps with a height of 0.2 nm are present. Almost all

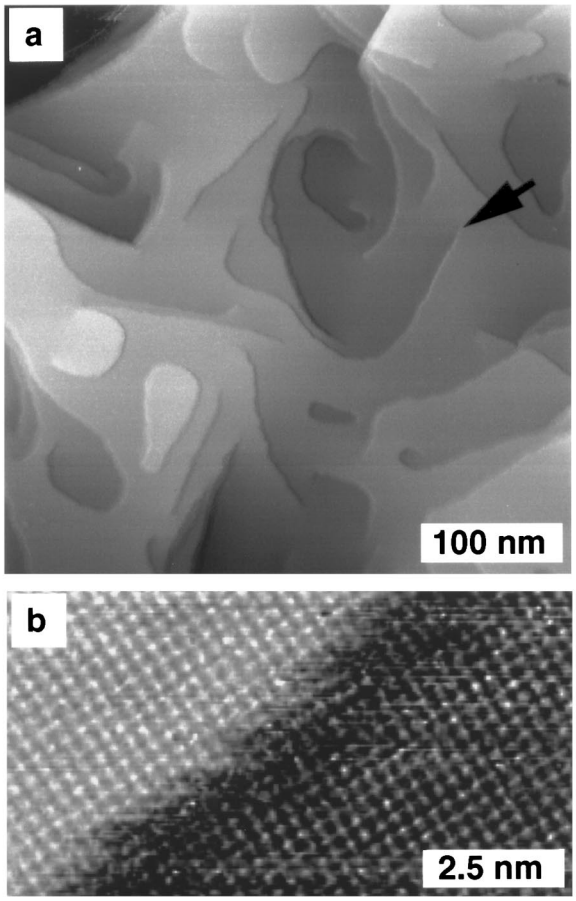

FIG. 2. STM images of a Ag(001) substrate grown as buffer layer on Fe-precovered GaAs(001): (a) Overview image (400×400 nm^2; vertical range: 2 nm), (Ref. 16), (b) atomically resolved area across a step edge (9.7×5.3 nm^2; vertical range: 0.3 nm).

of them originate from screw dislocations (e.g., black arrow), which is the most numerous type of defect occurring on these substrates. We believe this is due to the underlying faceted GaAs surface.[15] The total height variation from the lowest to the highest point (hereafter called *vertical range*) within a 400×400 nm^2 frame is only 2 nm, and the mean terrace width measures 36 nm. Atomically resolved images [Fig. 2(b)] of the Ag(001) lattice and a clear fourfold (1×1) LEED pattern [Fig. 3(a)] with sharp spots and a low background confirm the epitaxial growth mode. The step running across Fig. 2(b) appears fuzzy due to Ag adatoms diffusing

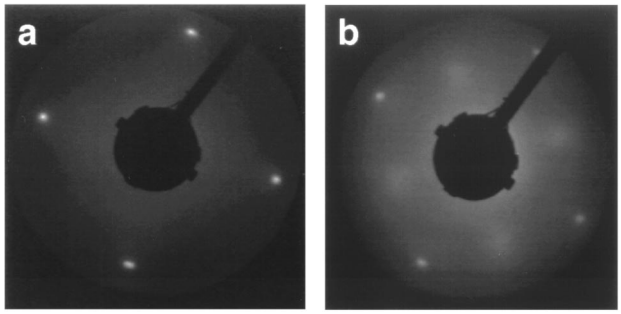

FIG. 3. LEED pattern taken at 50 eV of (a) a Ag(001) substrate and (b) an Fe(001) film grown at room temperature. The patterns are displayed with an arbitrary relative orientation.

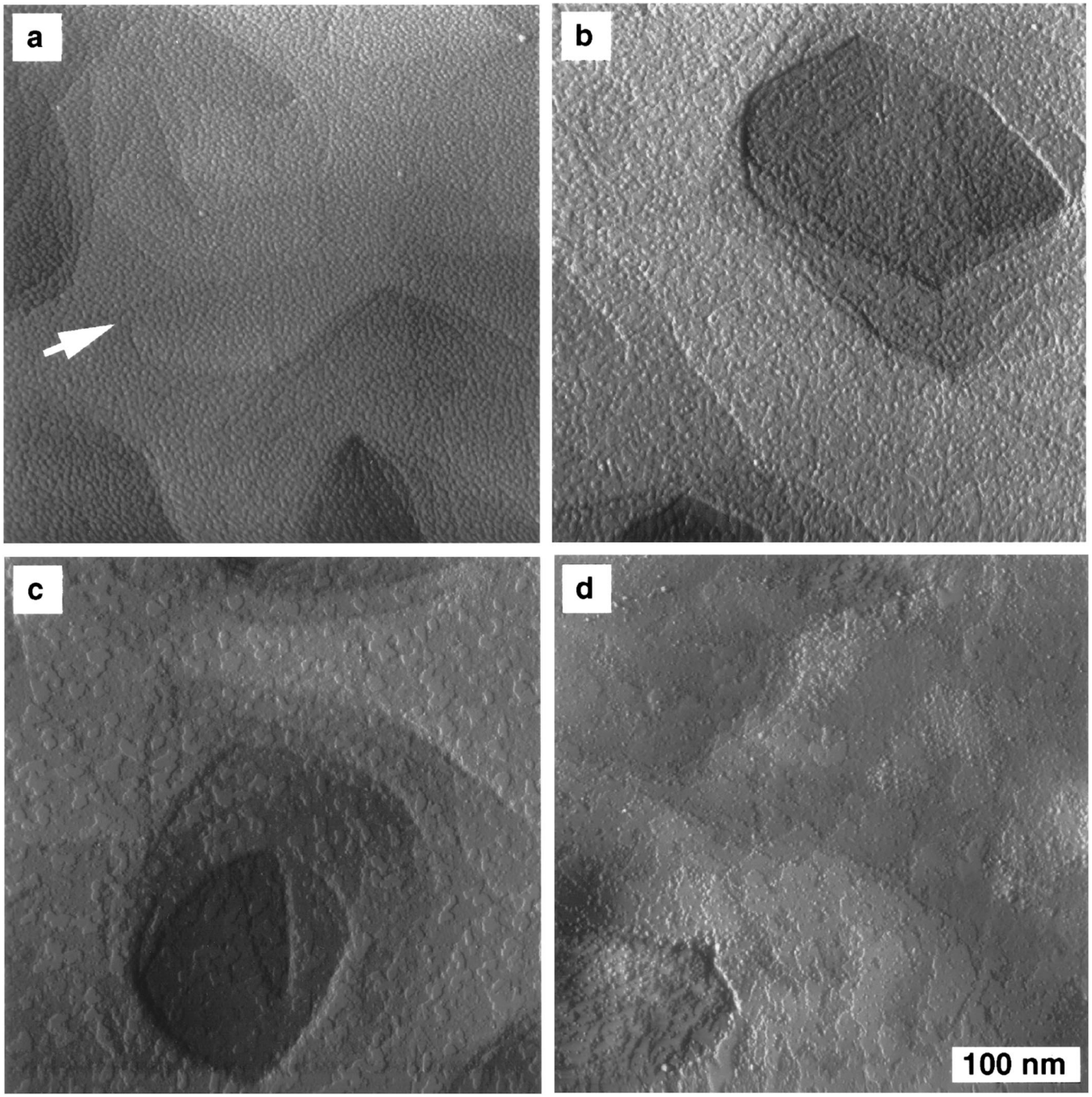

FIG. 4. Overview STM images of a RT Fe film before and after postannealing at increasing T_A (image size: 400×400 nm^2) (Ref. 16): (a) as-grown (vertical range: 4 nm), (b) postannealed at 520 K (vertical range: 3 nm), (c) postannealed at 600 K (vertical range: 2 nm), (d) postannealed at 670 K (vertical range: 2 nm).

along the step edge. This observation is a further confirmation of the cleanness as contaminants tend to decorate steps and thereby suppress step edge diffusion.[15]

IV. MORPHOLOGY OF Fe FILMS GROWN AT 300 K AND 520 K

An overview STM image of an RT Fe film is shown in Fig. 4(a).[17] The shape and arrangement of the substrate-induced steps is very similar to what we observe on the bare Ag(001) substrate [Fig. 2(a)]. Even screw dislocations can still be identified [white arrow in Fig. 4(a)]. Between two substrate-induced steps we do not find a single structureless flat terrace, instead the surface is covered by hillocks as revealed by the detail image in Fig. 5(a).[17] The surface roughness within a former substrate terrace is vertically characterized by the mean hillock height of about 1.0 nm (7 ML or 20% of the nominal film thickness) and laterally by the mean hillock separation of about 5 nm. Hereafter the mean hillock height measured as the total height range in areas of STM images $z(\boldsymbol{\rho})$ that are not disturbed by substrate-induced steps is called *roughness amplitude* and the mean separation between typical features is referred to as *roughness period*. It is determined by the position of the nearest-neighbor maximum in

TABLE I. Roughness period and amplitude (as defined in Sec. IV), and Ag coverage determined from XPS for samples grown according to four different growth procedures (RT, HT, LT, and MT) and the evolution of these quantities upon annealing. The fourth column additionally gives a qualitative description of the surface structures and the sixth one a reference to the corresponding STM images.

Preparation	Temperature	Roughness period	Roughness amplitude	Ag coverage	Figure
RT:	T_S=300 K	5 nm	~7 ML (hillocks)	~ 0.1 ML	4(a), 5(a)
	T_A=520 K	7 nm	3–4 ML (islands)	~ 0.1 ML	4(b), 5(b)
	T_A=600 K	25 nm	2–3 ML (islands)	~ 0.1 ML	4(c), 5(c)
	T_A=670 K	undefined	undefined	~ 0.4 ML (+Ga)	4(d), 5(d)
HT:	T_S=520 K	25 nm	6 ML (table mountains)	~ 1.0 ML	6
	T_A=570 K	25 nm	6 ML (table mountains)	~ 1.0 ML	
LT:	T_S=100 K	~5 nm	~7 ML (hillocks)	~ 0.04 ML	
	T_A=540 K	~7 nm	~7 ML (table mountains)	~ 0.04 ML	10
MT:	T_S=100/570 K	25 nm	4–5 ML (table mountains)	~ 0.02 ML	11

$$h(r)=\int_0^{2\pi} H(r,\vartheta)\,d\vartheta, \tag{1}$$

where

$$H(r,\vartheta)=H(\boldsymbol{r})=\int_A z(\boldsymbol{\rho})z(\boldsymbol{\rho}+\boldsymbol{r})\,d^2\rho \tag{2}$$

is the two-dimensional height-height correlation function. These quantities are summarized in Table I for all preparation procedures considered in this paper. Obviously, Fe grows on Ag(001) at room temperature as a continuous film with a rough surface. The (1×1) LEED pattern of this as-grown film [Fig. 3(b)] proves the single crystallinity and establishes the epitaxial relationship: the bcc-Fe(001)$\langle100\rangle$ axis is parallel to the fcc-Ag(001)$\langle110\rangle$ axis. The weak and broad spots with $c(2\times2)$ symmetry are most likely due to nitrogen adsorption from the residual gas as suggested by barely visible peaks in the AES and XPS spectra.

The evolution of the surface morphology upon postannealing at various temperatures is shown in overview and detail images (b)–(d) of Figs. 4 and 5. Upon postannealing at 520 K the hillocks have transformed into islands with clear steps resulting in a reduced roughness amplitude of 0.5 nm

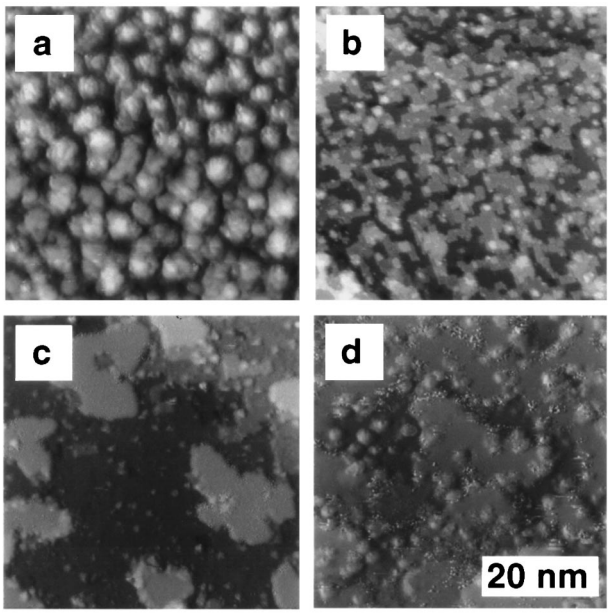

FIG. 5. Detail STM images of a RT Fe film before and after postannealed at increasing T_A (image size: 50×50 nm^2) (Ref. 16): (a) as-grown (vertical range: 1.0 nm), (b) postannealed at 520 K (vertical range: 0.6 nm), (c) postannealed at 600 K (vertical range: 0.6 nm), (d) postannealed at 670 K (vertical range: 0.5 nm).

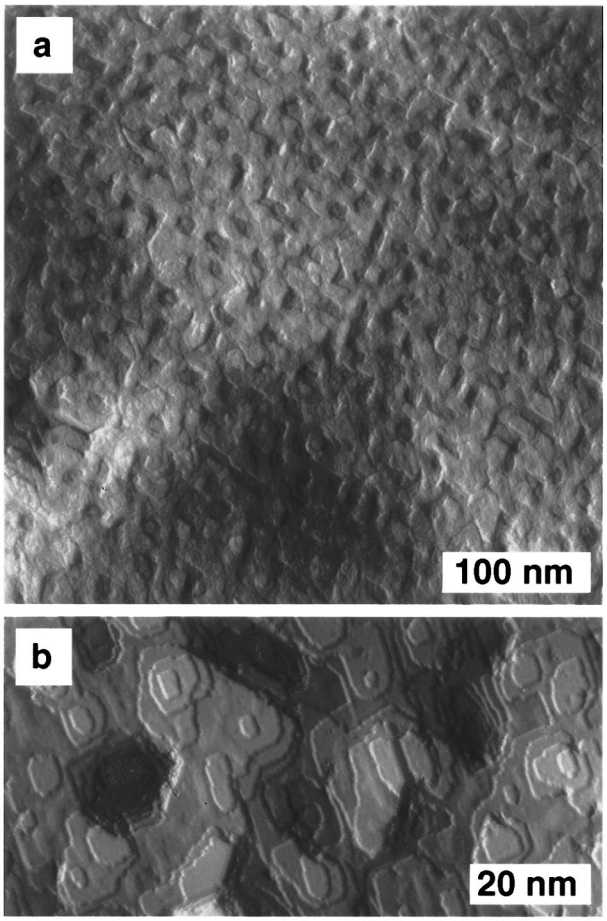

FIG. 6. STM images of a HT Fe film (Ref. 16): (a) overview image (400×400 nm^2; vertical range: 4.0 nm), (b) detail image (100×50 nm^2; vertical range: 1.0 nm).

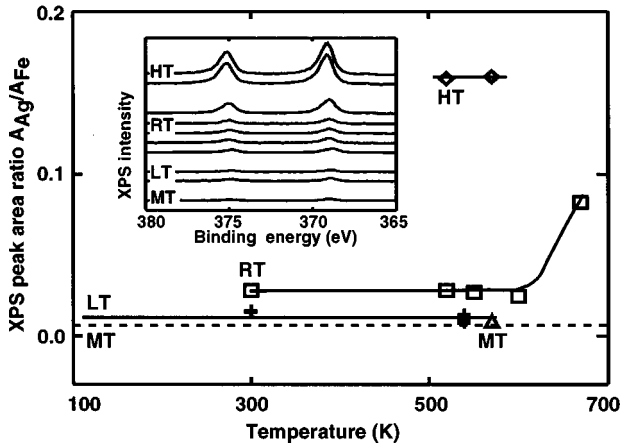

FIG. 7. Peak area ratio A_{Ag}/A_{Fe} as a function of temperature for samples grown at T_S=100/570 K (MT, △), T_S=100 K (LT, +), T_S=300 K (RT, □), and T_S=520 K (HT, ◇) derived from the XPS spectra shown in the inset. The dashed line indicates the theoretically expected value due to the Ag substrate. The positions of the labels MT, LT, RT, and HT mark the growth temperatures. All measurements are taken at room temperature after postannealing at temperatures as indicated by the symbols. The errors can be estimated from the scattering of the crosses in the LT case. Solid lines are guides to the eye. Inset: Evolution of the XPS Ag 3*d* lines normalized to the Fe 2*p* peak area upon annealing after growth at T_S=100/570 K (MT), T_S=100 K (LT, T_A=540 K), T_S=300 K (RT, T_A=520 K, 550 K, 600 K, and 670 K), and T_S=520 K (HT, T_A=570 K).

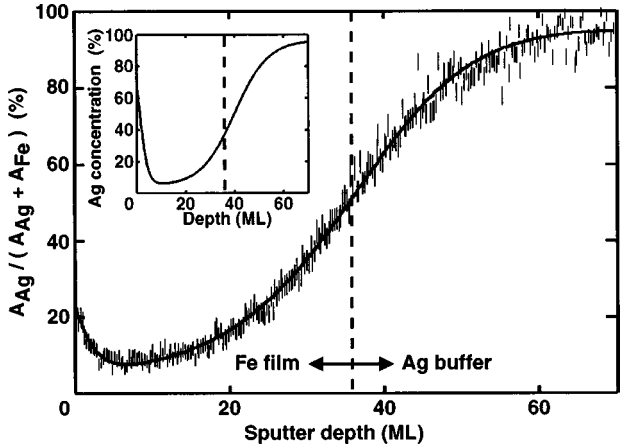

FIG. 8. Normalized XPS peak area as a function of the sputter depth measured for a HT Fe film. The error bars indicate the error due to count rate statistics. The solid line represents the fit to the experimental data yielding the Ag concentration profile $C_{Ag}(z)$ shown in the inset.

(3–4 ML). Each gray tone in Figs. 5(b) and (c) corresponds to a different atomic layer. The roughness period measured as the mean separation of the islands amounts to about 7 nm. Postannealing at 600 K leads to an even flatter surface with a decreased roughness amplitude of 0.4 nm (2–3 ML) and an increased roughness period of 25 nm. For the annealing cycles discussed up to now the large-scale morphology does not depend very much on annealing [Figs. 4(a)–(c)]. It still resembles the appearance of the Ag substrate. Upon postannealing at the highest temperature considered here (670 K), however, it changes dramatically. The substrate-induced step structure vanishes and the surface becomes inhomogeneous [Fig. 4(d)] revealing rather rough (e.g., lower left corner) and flat areas (e.g., lower right corner) next to each other. The flatter parts are similar in roughness as before the final annealing, but the edges of the islands seem to be decorated [Fig. 5(d)]. These STM images suggest that the sample has undergone intermixing or surface segregation. Chemical characterization as presented in Sec. V is necessary to confirm this suggestion.

Surfaces of Fe films grown at 520 K (HT) look differently compared to what we have discussed so far (Fig. 6). The substrate-induced steps no longer appear as sharp edges. They rather form a weak undulation of the surface with an amplitude of a few nanometers which is comparable to the vertical range measured on the substrate. The local surface structure consists of table mountains and holes with typical heights and depths of 3 ML yielding a roughness amplitude of 0.9 nm (6 ML) and a roughness period of about 25 nm. The step edges tend to run along two perpendicular axes reflecting the fourfold symmetry of the (001) surface. Postannealing at 570 K does not cause any changes in the STM images. The LEED patterns from these HT films are very similar to the one taken on the RT sample and shown in Fig. 3(b).

V. CHEMICAL PROPERTIES OF Fe FILMS GROWN AT 300 K AND 520 K

Rather high temperatures—during deposition or postannealing—were involved in the preparation procedure of the samples presented in the previous section. Since material transport processes, such as interdiffusion, segregation, or atomic exchange at the surface, may be activated at elevated temperatures it is worth checking the chemical composition of the surface layer.

The inset of Fig. 7 shows the evolution of the XPS Ag 3*d* peaks upon successively annealing of RT Fe films (five middle spectra) and HT Fe films (two topmost curves). The spectra are normalized with respect to the Fe 2*p* peak area. The main plot of Fig. 7 displays the peak area ratio A_{Ag}/A_{Fe} derived from these XPS spectra for various preparation procedures as a function of T_S and T_A, respectively. For samples grown at room temperature the Ag contribution (□) does not change upon annealing at temperatures up to 600 K whereas it is strongly increased after postannealing at T_A=670 K in which state we also measure clear Ga peaks indicating that the sample gets intermixed and thus confirming the suggestion derived from the STM data in Figs. 4(d) and 5(d). HT Fe films (◇) show about 6 times stronger Ag peaks than RT samples. Again, they do not change significantly upon annealing. With the Fe film thickness *d* being about 5 times the attenuation length of the Ag 3*d* photoelectrons the Ag contribution from the substrate is expected to be small and constant for all samples, and therefore it can definitely not explain the different peak area ratios of RT and HT samples. In order to quantify the theoretically expected substrate contribution we calculate the XPS peak areas of the Fe and Ag signals A_{Fe} and A_{Ag} using a continuum model:

$$A_{Fe}=s_{Fe}T_{Fe}\int_0^d \exp\left(-\frac{\zeta}{\lambda_{Fe}}\right)d\zeta, \tag{3a}$$

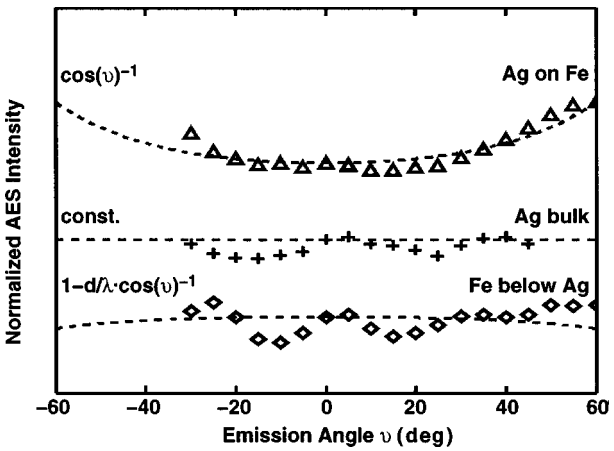

FIG. 9. AES intensity of Ag (△) and Fe (◇) as a function of the emission angle ϑ measured simultaneously on a HT Fe film. The middle curve (+) is taken on a clean, bulklike Ag(001) buffer layer for reference. The dashed curves show the expected behavior neglecting channeling and AED effects.

$$A_{\mathrm{Ag}} = s_{\mathrm{Ag}} T_{\mathrm{Ag}} \int_d^\infty \exp\left(-\frac{\zeta}{\lambda_{\mathrm{Ag}}}\right) d\zeta. \tag{3b}$$

Here, s_X are the XPS sensitivities given in Ref. 18, λ_X the photoelectron attenuation lengths,[19] and T_X the electron analyzer transmission probabilities for the Ag $3d$ and the Fe $2p$ lines, respectively. The theoretical peak area ratio $A_{\mathrm{Ag}}/A_{\mathrm{Fe}}$ due to the substrate contribution is about 4 times smaller than what we measure in the spectrum of the RT sample (compare dashed line and the curve labeled RT in Fig. 7, note the position of zero on the ordinate).

Summarizing these experiments we find that there must be Ag atoms at the surface or within the Fe layer contributing to the spectra. The amount of Ag visible in XPS additional to the substrate contribution depends on the growth temperature T_S but not on the postannealing temperature T_A up to $T_A = 600$ K. Where are the additional Ag atoms located?

In order to answer this question we perform depth profile analysis. We choose a low ion beam current density of about 1 μA cm^{-2} at 2.5 keV and a short sputter cycle duration of 100 s to achieve good depth resolution. The total sputter time accumulated over 270 cycles is 450 min and the final sputter depth about 70 ML. The evolution of the normalized XPS Ag peak area $A_{\mathrm{Ag}}/(A_{\mathrm{Ag}}+A_{\mathrm{Fe}})$ as a function of the sputter depth z is plotted in Fig. 8 for a HT Fe film. The signal drops within the first few sputter cycles from 20% to a minimum of 10% and then steadily increases while the Fe film is getting thinner and the surface is approaching the Ag substrate. The peak area ratio plotted in Fig. 8 does not directly correspond to the Ag concentration profile because XPS has a finite, photoelectron energy dependent probing depth of several ML.

We fit the experimental data according to the following model: The Ag concentration profile $C_{\mathrm{Ag}}(z)$ is assumed to consist of two nonabrupt interfaces, the first one corresponding to the transition from an Ag overlayer *on top* of the Fe film to the Fe film and the second one to the interface between the Fe film and the Ag buffer layer. An additive constant b accounts for Ag atoms *inside* the Fe film. Each interface is described by a Fermi function of the form

$$F(z,d,w) = \frac{1}{\exp\left(\dfrac{z-d}{w}\right)+1}, \tag{4}$$

where z is the depth and d the position of the interface, both measured from the original surface, and w is a measure for the interface width. The concentration profiles $C_{\mathrm{Ag}}(z)$ and $C_{\mathrm{Fe}}(z)$ are thus given by

$$C_{\mathrm{Ag}}(z) = a\{F(z,d_1,w_1)+[1-F(z,d_2,w_2)]\}+b, \tag{5a}$$

$$C_{\mathrm{Fe}}(z) = 1 - C_{\mathrm{Ag}}(z). \tag{5b}$$

The measured peak area $A_X(z)$ of element X at a depth z from the original surface must be written similarly to Eq. (3):

$$A_X(z) = s_X T_X \int_z^\infty C_X(\zeta) \exp\left(-\frac{\zeta - z}{\lambda_X}\right) d\zeta. \tag{6}$$

Fitting the ratio $A_{\mathrm{Ag}}(z)/[A_{\mathrm{Ag}}(z)+A_{\mathrm{Fe}}(z)]$ to the experimental data we obtain the parameters a, d_i, w_i, and b. The resulting Ag concentration profile [Eq. 5(a)] is shown in the inset of Fig. 8. The knowledge of the nominal Fe film thickness allows us to fix the position d_2 of the second interface (dashed line) and instead of d_2 we obtain the sputter velocity. It is constant over the whole thickness range if we assume equal sputter yields for Ag and Fe, otherwise we additionally have to fit the sputter yield ratio. The qualitative result of the fit does not depend on the assumption of equal sputter yields.

The depth of the first interface d_1 is about 1 ML and its width w_1 is between 1 and 2 ML. The interface between the Fe film and the Ag substrate w_2 is even wider; it measures 6–7 ML. It is important to mention that the interfaces appear wider than they actually are due to sputter-induced intermixing and surface roughening. Thus, we cannot obtain their intrinsic width from the depth profile. The constant Ag contribution b is fitted to be on the order of 5%. It is most likely that this is an artifact of sputter-induced intermixing because the Ag/Fe system is known to be immiscible in the bulk.[20]

The depth profile clearly shows that the Ag which is visible in the XPS spectra additional to the substrate contribution is predominantly located at the surface of the Fe film. This allows us to quantify the spectra shown in Fig. 7 by considering a three-layer model: a semi-infinite Ag substrate, 35 ML (5 nm) Fe, and a thin Ag overlayer of thickness d. We find $d_{\mathrm{RT}} \approx 0.1$ ML and $d_{\mathrm{HT}} \approx 1$ ML for samples grown at room temperature and 520 K, respectively (Table I). From the latter value it follows that the surface imaged in Fig. 6 is an Ag-covered Fe film.

This result is qualitatively confirmed by angle-resolved AES which in contrast to depth profiling is a nondestructive method with much lower influence on the sample structure. Data from a HT Fe film is displayed in Fig. 9. Triangles (△) show the normalized AES Ag intensity $I_{\mathrm{Ag}}(\vartheta)$ as a function

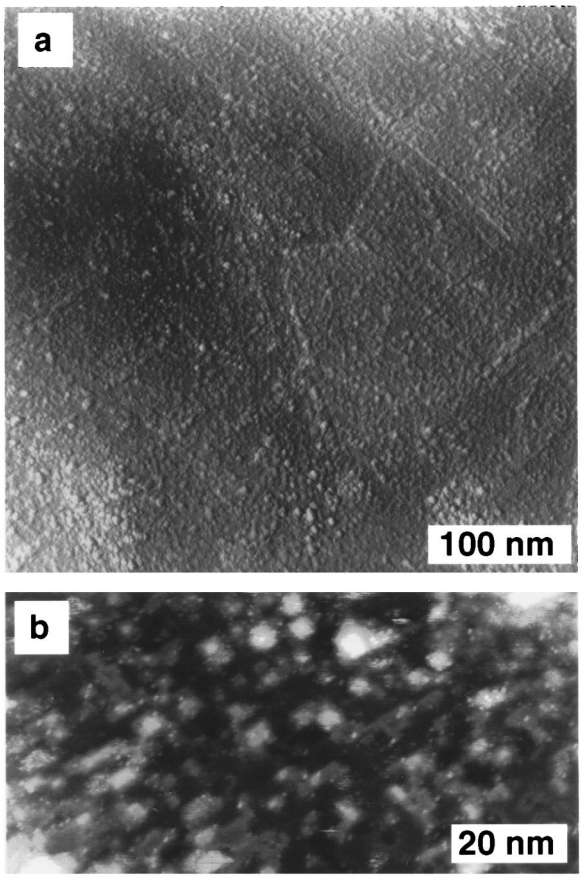

FIG. 10. STM images of a LT Fe film postannealed at 540 K (Ref. 16): (a) overview image (400×400 nm^2; vertical range: 2.0 nm), (b) detail image (100×50 nm^2; vertical range: 1.0 nm).

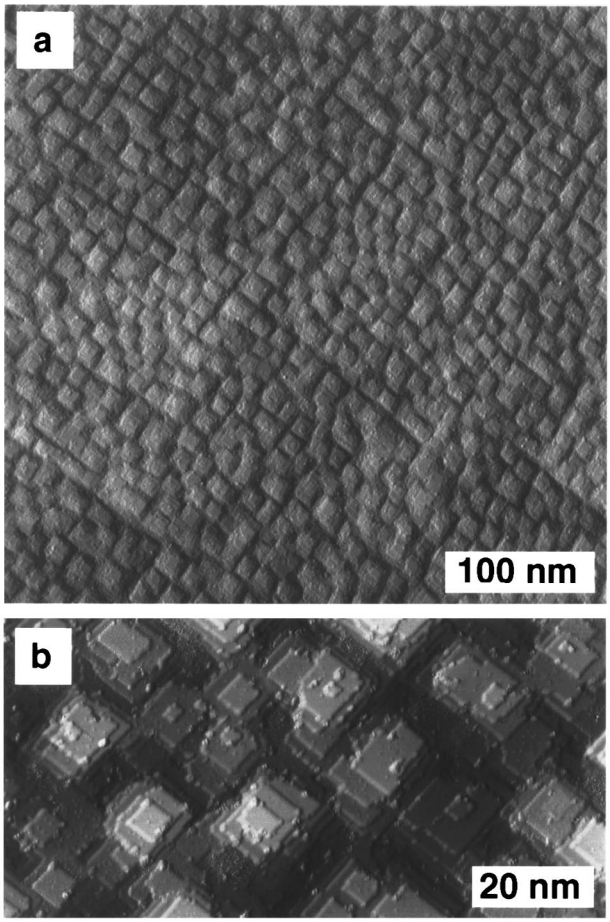

FIG. 11. STM images of a MT Fe film grown at 100/570 K (Ref. 16): (a) overview image (400×400 nm^2; vertical range: 2.0 nm), (b) detail image (100×50 nm^2; vertical range: 1.0 nm).

of the emission angle ϑ measured with respect to the surface normal and diamonds ($\diamond$) the normalized AES Fe signal $I_{\mathrm{Fe}}(\vartheta)$ which is recorded simultaneously. For a thin overlayer with thickness d these signals behave in the first order approximation in (d/λ) as $I_{\mathrm{Ag}}(\vartheta)\propto\cos(\vartheta)^{-1}$ and $I_{\mathrm{Fe}}(\vartheta)\propto1-(d/\lambda)\cos(\vartheta)^{-1}$, respectively. These functions are plotted as dashed lines under the assumption $d=1$ ML ($\lambda=6$ ML for the Fe LMM line). As our samples are single crystalline we have to make sure that the observed angular dependencies do not originate from channeling effects of the incident electrons or from Auger electron diffraction (AED). Therefore we perform a test experiment with a 150-nm-thick Ag(001) buffer layer [crosses (+) in Fig. 9]. Small deviations from the horizontal line—comparable in size and form with the waviness of the Fe signal ($\diamond$)—reflect channeling and AED effects. The much stronger angular dependence of the topmost curve verifies the presence of a thin Ag overlayer.

VI. OPTIMIZED GROWTH OF Fe FILMS

An optimized growth procedure must prevent Ag atoms from moving to the top of the growing Fe film and at the same time provide a well defined surface with minimized roughness amplitude and maximized roughness period. The data in Fig. 7 shows that the amount of Ag at the surface is reduced with decreasing growth temperature T_S. Obviously, room temperature is not low enough to completely suppress the Ag segregation at the surface. This demands for even lower deposition temperatures. On the other hand, elevated temperatures tend to smooth out the surface (Figs. 4–6).

For these reasons we grow Fe at 100 K (LT) achieving a rather rough surface comparable to Figs. 4(a) and 5(a). The amount of Ag in the XPS spectrum is only slightly higher than what we expect theoretically due to the Ag substrate [see crosses (+) in Fig. 7], and it is unchanged upon annealing at temperatures as high as 540 K. Using the analysis described in Sec. V we obtain an Ag coverage $d_{\mathrm{LT}}=0.04\pm0.04$ ML, which is significantly smaller than $d_{\mathrm{RT}}\approx0.1$ ML and $d_{\mathrm{HT}}\approx1$ ML. The absence of Ag at the very surface is further confirmed by the missing of Ag peaks in UPS and AES measurements (not shown) which are even more surface sensitive than XPS. Figure 10 shows the morphology of a LT film after postannealing at 540 K. It appears only slightly better than the morphology of RT films immediately after deposition. The irregular surface makes it difficult to extract a value for the roughness period which is estimated to be of the order of 7 nm. The roughness amplitude measures about 1 nm (7 ML). Accordingly, this procedure provides a means to grow Ag-free Fe films, but unfortunately their surfaces are morphologically ill defined.

Stimulated by the STM work of Stroscio *et al.*[21,22] who

reported clearly enhanced homoepitaxial growth quality of Fe for temperatures above 523 K, we finally employ the following ''mixed temperature'' (MT) growth procedure: (i) growing the first 2 nm at $T_S=100$ K and (ii) the following 3 nm at $T_S=570$ K. The first step is to prevent substrate atoms from moving to the surface yielding a clean, Ag-free, but rough substrate for the second growth step which is supposed to take advantage of the good Fe homoepitaxial growth quality at elevated temperatures. The efficiency of the first step is shown by the triangle ($\triangle$) in Fig. 7 and the lowest curve in the inset: MT films are as clean and as free of Ag as LT films. UPS and AES experiments again support this result. The STM images (Fig. 11) show a remarkably regular arrangement of equally sized quadratic table mountains. Their edges are perfectly aligned parallel to bcc-Fe(001)$\langle 100\rangle$ axes. The roughness amplitude and period measure 0.7 nm (4–5 ML) and 25 nm, respectively.

Finally, we want to mention that the LEED patterns of LT and MT films before and after postannealing are comparable to the one in Fig. 3(b) proving the epitaxial growth mode even at 100 K.

VII. DISCUSSION

Our chemical characterization of the RT and HT films in Sec. V clearly shows that a significant amount of Ag segregates at the surface at these growth temperatures. The evolution of the Ag content upon postannealing reveals that the degree of Ag coverage strongly depends on the deposition temperature T_S but not on the annealing temperature T_A, as long as T_A is kept below 670 K. This behavior can be explained by an atomic exchange process[23–26] that takes place in the topmost layer during deposition. The temperature being high enough that the atoms can diffuse to low-energy sites, this process occurs if the difference between the total free energies of an Fe overlayer and an Fe layer covered by Ag atoms

$$\Delta\gamma=\gamma_{\mathrm{Fe}}-\gamma_{\mathrm{Ag}}\mp\gamma_{\mathrm{int}} \tag{7}$$

is positive. γ_{Fe} and γ_{Ag} denote the surface free energies of Fe(001) and Ag(001), respectively, and γ_{int} is the interface free energy of the Fe/Ag(001) interface. The minus sign applies for the first Fe monolayer and the plus sign for all following layers. Using $\gamma_{\mathrm{Fe}}\approx 2\gamma_{\mathrm{Ag}}$ as given in Refs. 27–29 and $\gamma_{\mathrm{int}}\approx\gamma_{\mathrm{Ag}}/2$ taken from Ref. 30 we obtain for the first and the following Fe monolayers

$$\Delta\gamma\approx\frac{1}{2}\gamma_{\mathrm{Ag}}>0 \quad \text{and} \quad \Delta\gamma\approx\frac{3}{2}\gamma_{\mathrm{Ag}}>0, \tag{8}$$

respectively. Thus, a monolayer of Ag is forced to cover the first deposited atomic layer of Fe. The same exchange process occurs for all following layers of Fe deposited resulting in a thin layer of Ag atoms ''floating'' on the growing Fe film. This process is fully efficient at 520 K when the saturation coverage of 1 ML is reached. At room temperature the exchange process is partly kinetically hindered and yields a coverage of only 0.1 ML. It is to be expected that some of the Ag atoms get stuck inside the Fe film. As γ_{Cr} is only slightly smaller than γ_{Fe}, the same mechanisms apply to Cr grown on Ag(001) or Ag covered Fe(001).[31] In the context of magnetic interlayer coupling in the Fe/Cr/Fe/Ag(001) system the question arises how the Ag atoms inside the sandwich structure influence the coupling behavior. Ag atoms in the spacer layer could act as ''loose spins'' in the framework of Slonczewski's theory,[9] and they also add to the spacer layer thickness shifting the phase of the oscillating coupling curve. Furthermore, being impurity scatterers at the interface, the Ag atoms are expected to have an influence on the magnitude of the GMR effect.[32]

During postannealing cycles, however, the Ag atoms of the substrate are buried underneath 35 ML of Fe. They cannot move to the energetically more favorable positions at the surface because the immiscibility of the Ag/Fe system imposes a much too high energy barrier on the diffusion through the Fe layer. This explains the higher stability of the system against postannealing at elevated temperature compared to growing at elevated temperature.

This scenario has previously been described for the Fe/Ag system by Egelhoff[30] when interpreting x-ray photoelectron and Auger electron forward-scattering data. The higher efficiency of the atomic exchange process observed at cryogenic temperatures by Egelhoff most likely originates from the deposition rate he used which was about one order of magnitude smaller than in our case.

The change in morphology upon annealing of the RT films presented in Sec. IV demonstrates the usefulness of postannealing cycles for temperatures below 670 K at which temperature the whole system mixes. Knowing about the Ag atoms at the surface it is unclear how to separate in the STM images Ag structures ''floating'' on the Fe film from intrinsic Fe structures. So far it has not been possible to distinguish Ag and Fe by STM neither in voltage dependent scans nor in the spectroscopic mode. In the case of HT films the STM data has to be interpreted as the image of a closed Ag monolayer on top of the Fe film of interest. The island shapes appear smoother on the HT films (Fig. 6) than on the MT surfaces (Fig. 11). This might result from Ag step edge diffusion going on in the Ag overlayer of the HT sample.

The optimized recipe for the growth of Fe(001) on Ag(001) proposed and successfully tested in Sec. VI yields surfaces which are free of Ag and at the same time show a well defined morphology with equally sized table mountains in a remarkably well ordered arrangement. This regular structure is suitably described by a roughness period and a roughness amplitude, the quantities we have defined in Sec. IV to characterize the surface morphology. Obviously, the MT morphology is the one which is closest to the typically periodic roughness models used in theoretical calculations considering the effects of interface roughness on GMR or magnetic interlayer coupling.[8,10]

While the advantage of the MT films with respect to the chemical properties is obvious, the improvement in morphology seems to be small at first glance. The roughness period (or equivalently the terrace width) is not increased by orders of magnitude; it varies for all preparation procedures at most by a factor of five from 5 nm to 25 nm. However, one should compare these values to a relevant physical length scale for the magnetism of thin Fe films, as, for instance, the ''exchange length''[8] $\sqrt{A}/M_S\approx 7$ nm (A being the exchange stiff-

ness and M_S the saturation magnetization). This magnetic length scale lies in the range of roughness periods spanned by our samples. Changes of the magnetic properties are therefore expected for the different preparation procedures, independent of the Ag content at the interfaces. The strength of the biquadratic coupling of Fe-based triplelayers, for instance, calculated in the framework of the magnetic-dipole[10] or the fluctuation[8] mechanism is more than doubled when the roughness period is increased from 10 nm to 30 nm. In view of these considerations the morphological improvements achieved in this work are of great relevance for magnetic properties.

The comparison of the surface morphology observed by STM with results from other techniques—mainly diffraction techniques as x-ray diffraction (XRD) or electron diffraction (LEED, reflection high-energy electron diffraction)—is not straightforward for four reasons: (i) Each method has a different (coherent) field of view ζ over which averaging takes place when extracting morphological information. For conventional LEED ζ is about 10 nm whereas it may be several μm for XRD depending on the geometry. In STM ζ can be varied to some extent by changing the scan size. For the present work $\zeta \approx 100-400$ nm seems appropriate for the reasons discussed above. (ii) Very often the roughness of an interface is characterized solely by its rms roughness $\sigma_{\mathrm{rms}} = \sqrt{\langle z^2 \rangle}$. This quantity lacks the important information about the lateral extent of the structures causing the roughness. This is best demonstrated by calculating σ_{rms} for an as-deposited RT and a MT Fe film from the STM images [Figs. 5(a) and 11(b)]. We obtain $\sigma_{\mathrm{rms}}^{\mathrm{RT}} = 0.209$ nm and $\sigma_{\mathrm{rms}}^{\mathrm{MT}} = 0.206$ nm (100 nm $\times$ 50 nm image size and 0.1 nm scan resolution in both cases) in spite of the roughness periods differing by a factor of five. (iii) STM images reveal the shape of the surface features and their mutual arrangement. This kind of information is hardly accessible by other techniques. (iv) STM is restricted to surfaces whereas, for example XRD has access to buried interfaces. In spite of these restrictions we want to compare our results to a comprehensive XRD study of Fe/Cr(001) superlattices deposited on Ag(001)/Fe/GaAs(001) substrates reported by Schreyer *et al.*[33] Samples grown at room temperature and at 520 K (HT) were measured under different scattering geometries yielding rms roughnesses σ_{rms} and lateral roughness coherence lengths ξ *averaged over all Fe/Cr interfaces occurring in the superlattice with 5–9 Fe/Cr repetitions*. σ_{rms} was found to be about 0.35 nm (2.5 ML) in HT samples and slightly increasing with the growth temperature. This is in fairly good agreement with our results ($\sigma_{\mathrm{rms}}^{\mathrm{HT}} = 0.270$ nm and $\sigma_{\mathrm{rms}}^{\mathrm{RT}} = 0.209$ nm). The uncorrelated coherence length ξ, which has to be compared to the roughness period determined from the STM images, was about an order of magnitude larger for HT samples than for multilayers grown at room temperature. This is in reasonable agreement with the factor five found in this work, whereas the roughly estimated absolute value ($\xi \approx 200$ nm) clearly exceeds the largest roughness period of 25 nm observed in our experiments.

Interestingly, all films which have been exposed to elevated temperatures above 540 K, either during deposition or during postannealing, tend to exhibit a roughness period on the order of 25 nm (Table I) suggesting this length to be intrinsic for thermally equilibrated Fe(001) films on Ag(001). The lattice mismatch $m = (a_{\mathrm{Ag}} - a_{\mathrm{Fe}})/a_{\mathrm{Ag}}$ between Ag(001) and Fe(001) deduced from the bulk nearest-neighbor distances $a_{\mathrm{Fe}} = 0.287(0)$ nm and $a_{\mathrm{Ag}} = 0.289(2)$ nm is 0.8% yielding a mean dislocation separation of $a_{\mathrm{Fe}}/m \approx 38 \pm 12$ nm. Although this value is larger than our measured upper limit for the roughness period the explanation of the observed morphology to be due to strain relief is appealing because it explains in a straightforward way the high degree of order in the arrangement of the table mountains in the MT film. This interpretation implies that the MT growth procedure yields an optimized surface morphology because the strain-induced dislocation network is an intrinsic property of the Fe/Ag system for this film thickness.

Concluding we want to stress two general points: (i) When tailoring thin film structures one has to consider the chemical structure to the same extent as the morphological. Both may critically depend on the preparation parameters as we have shown for the case of Ag segregation and roughness. (ii) The surface quality (especially the roughness) of the Fe films obtained in this work is not as high as it is known from whiskers[34] which exhibit almost perfect surfaces with a terrace width as large as 1 μm. We believe that the surface quality of our samples is more representative for many thin film and multilayer systems, be it in the Fe/Cr system or in others. Thus, keeping in mind the possibility that the interfaces of a layered system look like the ones imaged here rather than like surfaces of whiskers might be a good thing to do, especially when one is trying to understand subtle structure-properties relationships.

ACKNOWLEDGMENTS

We thank J.A. Wolf for his help in the early stage of this project and H. Breitenstein for technical assistance and quick help in critical situations. Financial support from the Swiss National Science Foundation and the Swiss *Kommission zur Förderung der wissenschaftlichen Forschung* is gratefully acknowledged.

*Corresponding author. Electronic address: buergler@ubaclu.unibas.ch, FAX: +41 61 2673784.

[1] *Magnetism and Structure in Systems of Reduced Dimension*, Vol. 309 of *NATO Advanced Study Institute, Series B: Physics*, edited by R. F. C. Farrow *et al.* (Plenum Press, New York, 1993).

[2] *Ultrathin Magnetic Structures*, edited by J. A. C. Bland and B. Heinrich (Springer-Verlag, Berlin, 1994), Vols. I and II.

[3] P. A. Grünberg *et al.*, in *Magnetism and Structure in Systems of Reduced Dimension* (Ref. 1), Chap. 9, pp. 87–100.

[4] R. J. Hicken *et al.*, J. Appl. Phys. **78**, 6670 (1995).

[5] C. Roth, F. Hillebrecht, H. Rose, and E. Kisker, Phys. Rev. Lett. **70**, 3479 (1993).

[6] A. Schreyer *et al.*, Europhys. Lett. **32**, 595 (1995).

[7] J. A. Wolf *et al.*, J. Magn. Magn. Mater. **121**, 253 (1993).

[8] J. C. Slonczewski, Phys. Rev. Lett. **67**, 3172 (1991).

[9] J. C. Slonczewski, J. Appl. Phys. **73**, 5957 (1993).

[10] S. Demokritov *et al.*, Phys. Rev. B **49**, 720 (1994).

[11] A. Vega *et al.*, Phys. Rev. B **49**, 12 797 (1994).

[12] J. C. Slonczewski, J. Magn. Magn. Mater. **150**, 13 (1995).

[13] P. Zahn, I. Mertig, M. Richter, and H. Eschrig, Phys. Rev. Lett. **75**, 2996 (1995).
[14] We will use the abbreviations RT, HT, LT, and MT very strictly only to indicate the different growth temperatures of our Fe films.
[15] D. E. Bürgler *et al.*, Surf. Sci. **366**, 295 (1996).
[16] The derivative along the fast scan direction (horizontal axis) has been added to the raw data after plane subtraction for contrast enhancement.
[17] All overview STM images are equally scaled. The same applies to the detail images with the exception of Fig. 2(b).
[18] J. H. Scofield, J. Electron Spectrosc. Relat. Phenom. **8**, 129 (1976).
[19] M. P. Seah, in *Practical Surface Analysis*, edited by D. Briggs and M. P. Seah (Wiley, Sussex, England, 1990), Vol. 1, Chap. 5, pp. 201–255.
[20] *Binary Alloy Phase Diagrams*, edited by T. B. Massalski *et al.* (American Society for Metals, Metals Park, OH, 1986), pp. 24–26.
[21] J. A. Stroscio, D. T. Pierce, and R. A. Dragoset, Phys. Rev. Lett. **70**, 3615 (1993).
[22] J. A. Stroscio and D. T. Pierce, Phys. Rev. B **49**, 8522 (1994).
[23] S. D. Bader and E. R. Moog, J. Appl. Phys. **61**, 3729 (1987).
[24] D. A. Steigerwald, I. Jacob, and W. F. Egelhoff, Jr., Surf. Sci. **202**, 472 (1988).
[25] P. J. Schmitz, W.-Y. Leung, G. W. Graham, and P. A. Thiel, Phys. Rev. B **40**, 11 477 (1989).
[26] C. Nagl, E. Platzgummer, M. Schmid, and P. Varga, Phys. Rev. Lett. **75**, 2976 (1995).
[27] L. Z. Mezey and J. Giber, Jpn. J. Appl. Phys. **21**, 1569 (1982).
[28] W. R. Tyson and W. A. Miller, Surf. Sci. **62**, 267 (1977).
[29] J. R. Smith and A. Banerjea, Phys. Rev. Lett. **59**, 2451 (1987).
[30] W. F. Egelhoff, Jr., in *Structural Property Relationships for Metal/Metal Interfaces*, edited by A. D. Romig, D. E. Fowler, and P. D. Bristowe, MRS Symposia Proceedings No. 229 (Materials Research Society, Pittsburgh, 1991), p. 27.
[31] D. E. Bürgler *et al.* (unpublished).
[32] B. A. Gurney, D. R. Wilhuit, V. S. Speriosu, and I. L. Sandres, IEEE Trans. Magn. **26**, 2747 (1990).
[33] A. Schreyer *et al.*, Phys. Rev. B **52**, 16 066 (1995).
[34] D. T. Pierce, J. A. Stroscio, J. Unguris, and R. J. Celotta, Phys. Rev. B **49,** 14 564 (1994).